サイトを欠いているなど、構造上、機能上、著しい欠損があり、腫瘍血管の走行状態も、血流の流れも極めて不規則である。さらに、内皮細胞間の間隙も1〜5μ大きく開いている場合もあるという。つまり、細菌（1〜2μ）でさえも腫瘍部でより選択的に漏出するわけであり（5-7）、いわゆるリポゾームやミセル剤にとってはまことに透過しやすい状況である。従って、AT-IIで昇圧することによって、とくに腫瘍血管部を押し拡げて EPR 効果を高めることができる（2〜3倍）［図 4］。実際の臨床で我々は AT –II の静脈注入により全
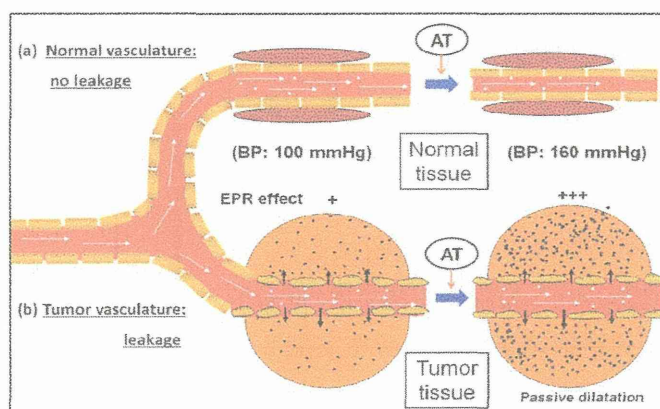

図4. Diagrammatic representation of the EPR effect and the effect of AT-II-induced hypertension accompanying the enhanced EPR effect and drug delivery in tumor tissue (b). Compare the effects in normal tissue (a). Under AT-II-induced hypertension (e.g. 100 → 160 mmHg), normal vessels and tumor vessels behaved differently. The normal blood vessels (a, right) have a smooth muscle cell layer that contracts and tightens the cell-cell junctions, and a narrowing of the vascular diameter that results in less drug leakage. In tumors (b), the vasculature endothelial cell-cell junctions open hydrodynamically (b, right). AT-II-induced hypertension thus leads to increased tumor-selective delivery of macromolecular drugs due to gap opening as demonstrated in clinical settings.

身血圧を昇圧状態になし、スマンクス/リピオドールを腫瘍栄養動脈内に注入するとデリバリーも上がり、薬効も大幅に改善することが可能になる。その結果はヒトの難治性の進行癌、例えば転移性肝癌、胆のう癌、腎癌、膵癌などの症例で証明されている（10）。

3. EPR 効果の定義とその周辺の問題

　　上記のような状況から腎排泄のない高分子（分子量約 4 万以上）であれば何でもよいかというとそうではない。例えば変性タンパク質や高度に化学修飾をほどこした血清タンパク質（IgG など）、あるいはα_2マクログロブリン（プロテアーゼ阻害タンパク）がプラスミン（プロテアーゼ）と E/I 複合体になったものなどは、もともと数日もある血中半減期は 5 分〜3hr ほどに激減する［表 2］。つまり、生体の異物認識機構により直ちに排除される。従って、これらを含めて生体親和性を EPR 効果の第一のパラメータとして挙げることができる［表 2〜4］。表 2、3 に示すように、いわゆる生体親和性がある高分子であることがまず優先される。

　　これら分子量や生体親和性に加えて、表面電荷の問題がある。ナノ粒子（タンパク、リポゾーム、ミセル、遺伝子を含む超微粒子）などにおいて、例えば、塩基性の強いポリカチオンでは、静脈内投与後、数分で血中から消失する。酸性度の強いポリアニオン（例えば表面荷電−40mV）などは肝、ついで脾に効率的に蓄積し、数十分〜数時間内に血中から消失する。一般に強い陽性荷電をもつポリマーは、血管内皮細胞表層におけるカルボキシレート基、サルフェート基などの負電荷が多く、強い陰性のため、血中半減期が極めて

3

短い［図5］。

　EPR 効果は早い場合には約十分でもみられるが（マウス）、血中濃度が長期間、高く維持されるとその間に炎症/癌局所で漏出・蓄積は継続するので数時間以上のほうが好ましい。血管造影という X 線診断法では、低分子の血管造影剤を病巣局所を支配している栄養動脈内に投与すると、ほんの一過性（1～2 分以内）には腫瘍部で漏出し、X 線画像上には腫瘍が濃染して見えるが、水溶性・低分子の造影剤は自由拡散により、急速に消失する。これはいわゆる passive targeting である。これに対し、EPR では例えばリピオドール（油性造影剤）の動注では腫瘍部のみに何週（～数ヶ月）も滞留する。この間、スマンクスのように薬剤が徐放すれば効果（毒力）は癌部のみで持続し、副作用のない治療が可能となる（5,7,10）。
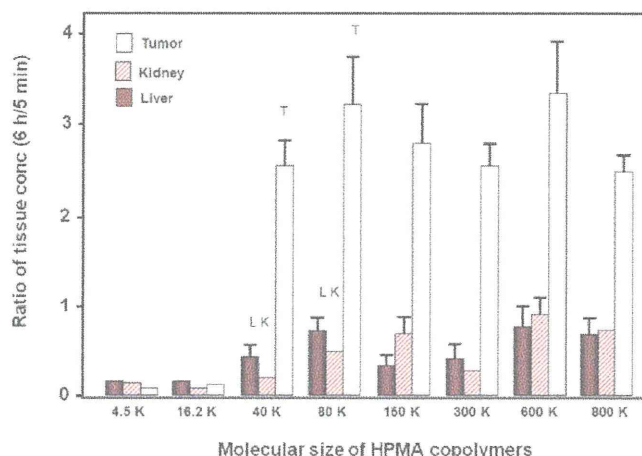

図5. Tumoritropic uptake of the biocompatible macromolecule *N*-(2-hydroxypropyl)methacrylamide (HPMA) polymer containing radioactive ^{131}I-labeled tyrosine. The EPR effect leading to higher uptake of the HPMA polymer into tumors is seen for polymer sizes larger than 40 kDa. The amount of uptake at 6 h is compared with that at 5 min. That is, tumor uptake increases with time.

表2　Characteristics needed for the EPR effect of nanomedicines and macromolecular drugs.

Biocompatibility	No interaction with blood components or blood vessels, no antigenicity, no clearance by the reticuloendothelial system, no cell lysis. Biologically inert.
Molecular size	Larger than 40 kDa (larger than the renal clearance threshold).
Surface charge	Weakly negative to near neutral.
Time required to achieve	Longer than several hours in systemic circulation in mice, with distinct accumulation seen at 30 min.
Drug retention time	Usually days to weeks, in great contrast to passive targeting, in which low-molecular-weight contrast imaging agents are rapidly accumulate in tumor, but cleared by diffusion into the systemic circulation in a few minutes.

[a] Compare with low-molecular-weight contrast agents in angiography, which is taken up in the tumor tissue by passive targeting, but not retained. Arterial injection of low molecular weight anticancer agents, though they hit tumor by the first path effect, is not retained in tumor tissue, and so not much benefit clinically.

4

表 3　Plasma clearance times of selected modified and native proteins *in vivo*.[a]

Proteins	Species difference, original/test	Probe modification	pI	MW (kDa)	$t_{1/2}$
Albumin	Mouse/mouse	None	4.8	68	72–96 h
	Mouse/mouse	DTPA (^{51}Cr)	≤4.8	—	6 h
	Cow/mouse	DTPA (^{51}Cr)	≤4.8	—	1 h
Formaldehyde-modified albumin	Human/rat	^{125}I-labeled formaldehyde	≤4.8	—	25 min
α_2-*Macroglobulin*	Human/mouse	[125]I	5.3	180×4	140 h
α_2-Macroglobulin-plasmin complex	Human/mouse	[125]I	—	180×4	5 min
Interferon (IFN-α)	Human/human	None	—	18	8 h (sc)
PEG-IFN-α2a	Human/human	PEG	—	52	80 h (sc)

[a]DTPA, diethylenetriaminepentaacetic acid; IFN, interferon; PEG, polyethylene glycol; sc, given subcutaneously. (Data modified from ref. 12 (a) and (b))

表　4　Surface charge affecting plasma residence times of different nanoparticles in mice.

Type of nanoparticles	ζ potential (mV)	Mean particle size (nm)	Plasma residence time		Remarks
			$T_{1/2}$	$T_{1/10}$	
Liposome					
Non-PEGylated	-7.31	124	9.08 h	>24 h	Doxorubicin loaded, DPPC:Chol = 1:1
Weakly cationic	+5.58	131	4.51 h	15 h (mean)	Doxorubicin loaded, DPPC:Chol:DC-Chol = 5:4:1, slightly positive
Strongly cationic	+24.25	95	<30 min	<10 min	Doxorubicin loaded, DPPC:DC-Chol = 5:5, strongly positive
Poly-L-Lys/DNA	Positive	—	<5 min	30 min	^{32}P-labeled 8-kbp DNA
Chitosan nanoparticle					
Weakly anionic	-13.2	149.2	—	12 h (mean)	CM/MM = 1:2, slightly negative
Strongly anionic	-38.4	156.0	—	3 h (mean)	CM/MM = 2:1, strongly negative
Weakly cationic	+14.8	150.1	—	<1 h	CH/MM = 1:1, slightly positive
Strongly cationic	+34.6	152.7	—	<1 h	CH/MM = 2:1, strongly positive

DPPC, dipalmitoylphosphatidylcholine; Chol, cholesterol; CM, carboxymethyl chitosan; MM: methyl methacrylate polymer.　(Data modified from ref. 13)

5．EPR 効果と蛍光ナノプローブによる腫瘍の蛍光イメージングと PDT（光照射療法）

　　当初、我々は EPR 効果を肉眼的にエバンスブルーアルブミンによる腫瘍部の選択的に濃染像として確認し、さらにより普遍的に合成高分子で生体親和性の極めて高い HPMA（ヒドロキシプロピルメタアクリレート）ポリマーにチロシンを導入し、その放射性ヨード化物を用いてより放射能のカウントにより系統的に数値化してその詳細をみた（2,3,4）。

　　最近、同じことをローダミンイソチオシアネート（RITC）標識アルブミンを用いて担癌（S-180）マウスの系で検討したところ、フリーの低分子ローダミン B（MW479.1）では全く腫瘍集積性がないのに対し、RITC-BSA（分子量約 7 万）は鮮明な腫瘍の蛍光像を呈した。蛍光画像イメージング装置 IVIS により、正常部よりも腫瘍部は 10 倍以上の蛍光を発していた。我々はこれを内視鏡装置に応用し、内視鏡による蛍光検出を施行することに

よって、超早期癌の検出を目指した研究を展開している。

　　一般に、光照射療法は He/Ne レーザー光線（出力波長 635nm）により励起した蛍光プローブから、一重項酸素を発し、殺細胞作用になるが、今回、内視鏡のキセノン光源でも 2〜3cm 以上の深度に充分な組織透過性を示し、HPMA-ZnPP の場合、光照射によってはじめて著明な抗腫瘍効果がみとめられた。この場合、EPR 効果による蛍光増感ナノプローブの腫瘍選択的集積を可能にし、その蛍光部（腫瘍部）のみの可視光の照射でその局所のみのピンポイントな治療ができるという点で、将来、管腔臓器（例えば口腔、食道、胃、腸、膀胱、子宮、腹腔、胸腔、気管支、尿道など、および肉腫や皮膚癌などの表層癌）等への広範な応用が期待される。これはまた、従来の低分子蛍光増感プローブが全身に分布し。日常の明るさでも皮膚に障害を与えるのに対し、この HPMA-ZnPP では腫瘍選択性が高いので、皮膚障害はみられない。

6. 結び

　　EPR 効果発見 26 年になるが、スマンクス以外に近年、ようやくリボゾーム製剤、ミセル製剤、抗体薬などの高分子制癌剤の第一世代のプロトタイプ型抗癌剤が認識されてきた。ここ 10-20 年の間に、活性本体の release 制御（pH、プロテアーゼ sensitive により可能）、血中動態（長い $t_{1/2}$）、癌組織内の浸透性等の個々の問題点が理解されるようになり、図 6 に示す各ステップに対し、夫々の方策が明らかとなってきた。いよいよこれからが高分子型製剤の出番である。蛍光イメージングはまさに EPR 効果の証明そのものであり、上記の ZnPP ポリマー製剤は今後、蛍光内視鏡を用いたいわゆる Theranostics のさきがけとなることを願っている。このようなナノプローブによる早期発見とその PDT による早期治療は、まさにその一石二鳥を可能にしようとするものである。

Steps	Barriers to be overcome	Comments
1st	Vascular wall/Circulating Blood EPR effect/Extravasation into tumor tissue Tumor tissue/interstitial space	Polymeric drugs/nanomedicines Vascular wall openings Enhancement of the EPR effect by NO and angiotensin-converting enzyme inhibitor
2nd	Dissemination to tumor cells	Stromal matrix/fibrin gel/fibroblast: protease/plasmin/plasminogen activator
3rd	Cell membrane/internalization	Endocytic uptake Styrene-co-maleic acid (SMA) micelle disintegration
4th	Drug release/free active drug pH/protease-labile linker Interact with target molecules	No reverse exocytosis Hydrazone/maleic acid
5th	In vivo antitumor effect: 100% survival/cure	React with target molecules High antitumor efficacy in vivo
6th	Regulatory steps/safety issue	Phase I, II, III trials
7th	Cost/benefit	More universal tumor targets [Evaluation by Natl. Inst. Health Clin. Excellence, UK]

図6. Barriers to the development of macromolecular drugs for cancer and steps to be overcome.

6

8．参考文献

(1) V. Torchilin, Tumor delivery of macromolecular drugs based on the EPR effect, Adv. Drug Deliv. Rev. 63, 131-135 (2011).

(2) Y. Matsumura and H. Maeda: A new concept for macromolecular therapeutics in cancer chemotherapy: Mechanism of tumoritropic accumulation of proteins and the antitumor agent SMANCS. Cancer Res., 46, 6387-6392 (1986)

(3) Y. Noguchi, J. Wu, R. Duncan, J. Strohalm, K. Ulbrich, T. Akaike and H. Maeda: Early phase tumor accumulation of macromolecules: A great difference in clearance rate between tumor and normal tissues. Jpn. J. Cancer Res., 89, 307-314 (1998)

(4) H. Maeda, J. Wu, T. Sawa, Y. Matsumura and K. Hori: [Review] Tumor vascular permeability and the EPR effect in macromolecular therapeutics. J. Cont. Release, 65, 271-284 (2000)

(5) H. Maeda, T. Sawa, and T. Konno: Mechanism of tumor-targeted deliverly of macromolecular drugs, including the EPR effect in solid tumor and clinical overview of the prototype polymeric drug SMANCS. J. Cont. Release, 74, 47-61 (2001)

(6) H. Maeda: Tumor-selective delivery of macromolecular drugs via the EPR effect: Background and future prospects, Bioconj. Chem. 21, 797-802 (2010)

(7) H. Maeda: Vascular permeability in cancer and infection as related to macromolecular drug delivery, with emphasis on the EPR effect for tumor-selective drug targeting. Proc. Jpn. Academy, Series B. 88, 53-71 (2012)

(8) H. Maeda, Y. Matsumura and H. Kato: Purification and identification of [hydroxyprolyl3] bradykinin in ascitic fluid from a patient with gastric cancer. J. Biol Chem., 263, 16051-16054 (1988)

(9) H. Maeda, Y. Noguchi, K. Sato and T. Akaike: Enhanced vascular permeability in solid tumor is mediated by nitric oxide and inhibited by both new nitric oxide scavenger and nitric oxide synthase inhibitor. Jpn. J. Cancer Res., 85, 331-334 (1994)

(10) A. Nagamitsu, K. Greish, H. Maeda, Elevating blood pressure as a strategy to increase tumor targeted delivery of macromolecular drug SMANCS: Cases of advanced solid tumors, Japan. J. Clinical Oncol. 39, 756-766 (2009)

(11) J. Wu, T. Akaike and H. Maeda: Modulation of enhanced vascular permeability in tumors by a bradykinin antagonist, a cyclooxygenase inhibitor, and a nitric oxide scavenger. Cancer Res., 58, 159-165 (1998)

(12) (a) H. Maeda, Y. Matsumura, T. Oda and K. Sasamoto: Cancer selective macromolecular therapeutics: Tailoring of an antitumor protein drug. In Protein Tailoring for Food and Medical Uses (eds: R.E. Feeney and J.R. Whitaker), Marcel Dekker, Inc., New York-Basel, p. 353-382 (1986)

   (b) K. Greish, J. Fang, T. Inuzuka, A. Nagamitsu and H. Maeda: Macromolecular anticancer therapeutics for effective solid tumor targeting: Advantages and prospects. Clinical Pharmacokinetics, 42, 1089-1105 (2003)

(13) C. He, Y. Hu, L. Yin, C. Tang, and C. Yin, Effects of particle size and surface charge on cellular uptake and biodistribution of polymeric nanoparticles," Biomaterials, 31, 3657–3666 (2010).

Tumor targeting polymeric drugS based on the EPR effect; Its augmentation for drug delivery and efficacy, and extention to tumor imaging

Hiroshi Maeda

*Research Institute of Drug Delivery System, Sojo University*

Ever since the beginning of cancer chemotherapy, the major problem has been severe toxicity of anticancer drugs; the first reason for this matter is that toxic anticancer drugs affect both normal cells and tumor cells similarly. Second reason is that these drugs will be distributed either tumor or normal tissue indiscriminately.

We realized that solid tumor has quite different blood vessels anatomically and pathologically. When the biocompatible macromolecules are injected intravenously, they leak out much more into the tumor; i.e. vascular permeability is enhanced in tumor. Furthermore, the macromolecules thus extravasated into the tumor will be retained there for a long time (to weeks). This phenomenon was coined "the enhanced permeability and retention (EPR) effect" of macromolecules, which is applicable to the molecular size > 40 KDa.

In diversified tumors in vivo, however, they exhibit heterogeneity in the EPR effect that would result in inconsistent tumor drug delivery, and result in therapeutic failure. We now found ways to overcome this heterogeneity of EPR effect by using NO releasing agents (eg. nitroglycerin), angiotensin converting enzyme inhibitor, angiotensin II induced hypertension and others.

Thus, EPR effect based nanomedicine for cancer would offer us the first rational ways to the development of tumor targeted drugs. This will not only provides better therapeutic opinion, but also can be extend to the tumor imaging using fluorescent nanoprobes for selective visualization of tumor. We now developed fluorescent nanoprobes for endoscopic tumor detection about which we will report in this meeting. These nanoprobes can be changed to generate singlet oxygen [$^1O_2$] upon light irradiation. Consequently, one can achieve detection and treatment simultaneously by [$^1O_2$] as cytotoxic principle thus generated only at the tumor site.

<Reference>   H. Maeda, *Proc. Jpn. Academy, Series B.* 88, 53-71 (2012)
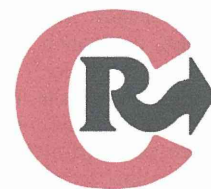
Micelles of zinc protoporphyrin conjugated to *N*-(2-hydroxypropyl)methacrylamide (HPMA) copolymer for imaging and light-induced antitumor effects in vivo

Hideaki Nakamura [a,b], Long Liao [a], Yuki Hitaka [a], Kenji Tsukigawa [a], Vladimir Subr [c], Jun Fang [a,b], Karel Ulbrich [c], Hiroshi Maeda [a,*]

[a] *Research Institute for Drug Delivery System, Faculty of Pharmaceutical Science, Sojo University, Kumamoto, Japan*
[b] *Laboratory of Microbiology and Oncology, Faculty of Pharmaceutical Science, Sojo University, Kumamoto, Japan*
[c] *Institute of Macromolecular Chemistry, Academy of Sciences of the Czech Republic, Prague, Czech Republic*

ARTICLE INFO

ABSTRACT

We synthesized *N*-(2-hydroxypropyl)methacrylamide polymer conjugated with zinc protoporphyrin (HPMA-ZnPP) and evaluated its application for tumor detection by imaging and treatment by light exposure using in mouse sarcoma model. To characterize HPMA-ZnPP micelle, we measured its micellar size, surface charge, stability, photochemical, biochemical properties and tissue distribution. In vivo anti-tumor effect and fluorescence imaging were carried out to validate the tumor selective accumulation and therapeutic effect by inducing singlet oxygen by light exposure. HPMA-ZnPP was highly water soluble and formed micelles spontaneously having hydrophobic clustered head group of ZnPP, in aqueous solution, with a hydrodynamic diameter of 82.8 ± 41.8 nm and zeta-potential of $+ 1.12$ mV. HPMA-ZnPP had a long plasma half-life and effectively and selectively accumulated in tumors. Although HPMA-ZnPP alone had no toxicity in S-180 tumor-bearing mice, light-irradiation significantly suppressed tumor growth in vivo, similar to the cytotoxicity to HeLa cells in vitro upon endoscopic light-irradiation. HPMA-ZnPP can visualize tumors by fluorescence after i.v. injection, which suggests that this micelle may be useful for both tumor imaging and therapy. Here we describe preparation of a new fluorescence nanoprobe that is useful for simultaneous tumor imaging and treatment, and application to fluorescence endoscopy is now at visible distance.

© 2012 Elsevier B.V. All rights reserved.

1. Introduction

Photodynamic therapy (PDT) employs a photosensitizer and cytotoxic light-induced singlet oxygen ($^1O_2$) generation. $^1O_2$ generation damages DNA, RNA, proteins and lipids, which leads to cell death. Porphyrin derivatives usually generate cytotoxic $^1O_2$ after light irradiation that corresponds to the absorption wavelength of porphyrin derivatives [1–3]. Laserphyrin® and Photofrin® and others are well known porphyrin derivatives that are approved for limited use in conventional clinical PDT for early-stage lung (bronchogenic) or superficial cancer accessible to exciting light (laser irradiation at 630 nm) [4,5]. However, small molecular photosensitizers are expected to be distributed throughout the body including skin and other organs, and most have limited tumor selectivity or tumor-imaging capacity. Thus, they would cause cutaneous hyper-photosensitivity as the major adverse effect, which limits therapeutic success.

To solve this problem, one can utilize macromolecular photosensitizers, which have much longer half-lives in circulation and gradually and selectively accumulate in tumor tissues because of the EPR

(enhanced permeability and retention) effect, accompanying much less accumulation in normal tissue [6–11]. Our group previously reported that biocompatible macromolecules (MW >40 kDa) showed the EPR effect and accumulated selectively in tumors [6,12,13]. For the EPR effect to operate, the macromolecular surface charge is as important a determinant as is molecular size; a neutral to slightly negative charge and MW of >40 kDa are preferable for tumor targeting [6,12,14]. In this study, we utilized a conjugate of zinc protoporphyrin (ZnPP) and 12-kDa *N*-(2-hydroxypropyl)methacrylamide (HPMA) copolymer, which has a neutral charge and is highly biocompatible. The conjugate behaved as a large macromolecule (apparent MW is 198-kDa), as do many polymer conjugates of low-molecular-weight micellar drugs that show preferential tumor accumulation [15–18].

Light-irradiated (at 420 nm, absorption max of ZnPP) ZnPP effectively generates $^1O_2$ and thereby exhibits potent cytotoxicity [18,19]. ZnPP is also a potent inhibitor of heme oxygenase-1 (HO-1), or HSP-32, which is a survival factor. HO-1 is highly upregulated in many cancer tissues in vivo and confers an antioxidative function to cells. Therefore, inhibition of HO-1 by ZnPP makes tumor cells more vulnerable to oxystress, the result being selective tumor regression. Most of normal cells are not affected because HO-1 in normal cells is expressed only at low level and insignificant. However, ZnPP is highly hydrophobic and soluble only in alkaline solutions or organic solvents. This

---

insolubility of ZnPP in physiological aqueous solution hampers its therapeutic application. To overcome this obstacle, we developed water-soluble ZnPP micelles: one is styrene maleic acid copolymer (SMA) micelles that encapsulate ZnPP and forms nanomicelles (SMA-ZnPP), the other is pegylated ZnPP (PEG-ZnPP) [18–22]. Both ZnPP micelles alone exhibited antitumor activity, and light irradiation greatly enhanced this activity [18]. Despite high tumor accumulation of PEG-ZnPP and significant antitumor activity, the maximum ZnPP loading in PEG-ZnPP is theoretically about 6% (wt/wt), so the intravenous (i.v.) dose of PEG-ZnPP may become several grams to achieve therapeutic concentrations. Although ZnPP loading of SMA-ZnPP can be increased to about 50%, SMA-ZnPP micelles tended to accumulate predominantly in the liver and spleen [23]. Therefore, we aimed to develop another type of ZnPP micelles with greater tumor targeting and adequate loading of ZnPP.

Here, we describe the synthesis of HPMA-ZnPP, which spontaneously formed micelles in aqueous solution. We examined its size distribution, spectroscopic property, micelle stability, generation of $^1O_2$, cellular uptake, tumor and tissue distribution and antitumor activity in vivo when used with xenon light-irradiation. Other important results concern simultaneous in vivo fluorescence imaging of the whole animal from outside, and the therapeutic effect of the polymer-photosensitizer conjugate.

2. Materials and methods

2.1. Materials

Male ddY mice were purchased from Kyudo Co., Ltd, Saga, Japan. Protoporphyrin IX, zinc acetate, triethylamine, dimethylaminopyridine, diethylether, Tween 20 and egg lecithin of reagent grade were purchased from Wako Pure Chemical, Osaka, Japan. 1-Ethyl-3-(3-dimethylaminopropyl)carbodiimide and 3-(4,5-dimethyl-2-thiazolyl)-2,5-diphenyl-2H-tetrazolium bromide (MTT) were purchased from Dojindo Chemical Laboratory, Kumamoto, Japan. 2,2,6,6-Tetramethyl-4-piperidone (4-oxo-TEMP) was purchased from Tokyo Chemical Industry, Tokyo, Japan. The HPMA polymer (mean MW ~12 kDa) we used contains one free amino group at the end, and was prepared at the Institute of Macromolecular Chemistry, Prague, Czech Republic.

2.2. Synthesis of HPMA-ZnPP

Scheme 1 shows the synthesis of HPMA-ZnPP conjugate, in which conjugation of carboxyl group of free ZnPP with either hydroxyl group or amino group of HPMA (mean MW 12 kDa) was carried out to form ester and amide bonds, respectively. In brief, 570 mg of HPMA as Scheme 1 and 281 mg of ZnPP were mixed in 50 ml of DMSO at 50 °C and reacted by addition of 1.0 g of triethylamine, 1.2 g of dimethylaminopyridine and 1.9 g of 1-ethyl-3-(3-dimethylaminopropyl)carbodiimide hydrochloride as a catalyst for 12 h at 50 °C in the dark. After the reaction, HPMA-ZnPP conjugates were precipitated by addition of diethylether (200 ml), and reaction catalyst in the supernatant was removed by centrifugation. The conjugates were washed three times with diethylether to remove the reaction catalyst and DMSO. HPMA-ZnPP was purified via gel permeation chromatography (Bio-Beads SX-1, BioRad, Hercules, CA) using dimethylformamide (DMF) as elute. Peak fraction of elutes was ultrafiltrated with membrane filter with a cutoff molecular size of 100 kDa, to remove decomposed or unreacted small molecules and to replace the DMF to distilled water. Fluffy powder (635 mg) was obtained by lyophilization.

2.3. Gel permeation column chromatography

Analytical gel permeation column chromatography of HPMA-ZnPP was performed with Bio-Beads SX-1 using a column ($\varphi = 2.5$ cm, L = 60 cm) and eluted with DMF at a flow rate of 0.1 ml/min. 1.5 ml

fractions of elutes were measured at absorbance at 422 nm, which corresponded to ZnPP absorbance.

2.4. Fluorescence spectroscopy and fluorescence polarization

HPMA-ZnPP at 10 μg/ml was dissolved in PBS containing Tween 20 (0.0005–0.5%) or urea (1–9 M), and fluorescence spectra were measured with a fluorescence spectrophotometer (FP-6600; JASCO, Tokyo). HPMA-ZnPP (2.5 μg/ml) or free ZnPP (0.5 μg/ml) was dissolved in DMF, and sample solutions were then excited at 420 nm by a fixed polarized light; fluorescence emission at 590 nm was recorded at parallel (0°) and perpendicular (90°) angles of the secondary polarizer, which was equipped in a Model FP-6600 fluorescence spectrophotometer. The fluorescence polarization value (P value) was calculated by using the equation $P = (I_{//} - I_\perp)/(I_{//} + I_\perp)$, where $I_{//} =$ fluorescence intensity of the parallel component and $I_\perp =$ fluorescence intensity of the perpendicular component. The fluorescent polarization value is proportional to the molecular size of the fluorescent probe [24].

### 2.5. High performance liquid chromatography (HPLC)

Cleavage of ester bond of this conjugate HPMA-ZnPP was analyzed by using HPLC (Prominence, Shimadzu, Kyoto, Japan) with the multimode size exclusion column GF-310 HQ (300 × 7.5 mm) with photodiode array detection at 422 nm, which was eluted with a mixture of 30% DMSO and 70% methanol containing 10 ppm trifluoroacetic acid at 1.0 ml/min.

2.6. Dynamic light scattering and zeta potential

HPMA-ZnPP or HPMA was dissolved in 0.01 M phosphate-buffered 0.15 M saline (PBS, pH 7.4) at 1 mg/ml and was filtered through a 0.2 μm filter attached to a syringe. The particle size and surface charge (zeta potential) were measured by light scattering (ELS-Z2; Otsuka Photal Electronics Co. Ltd., Osaka).

2.7. Transmission electron microscopy (TEM)

A drop of HPMA-ZnPP (0.1 mg/ml) was applied to a copper grid coated with carbon film and air-dried. The micelle image and size of
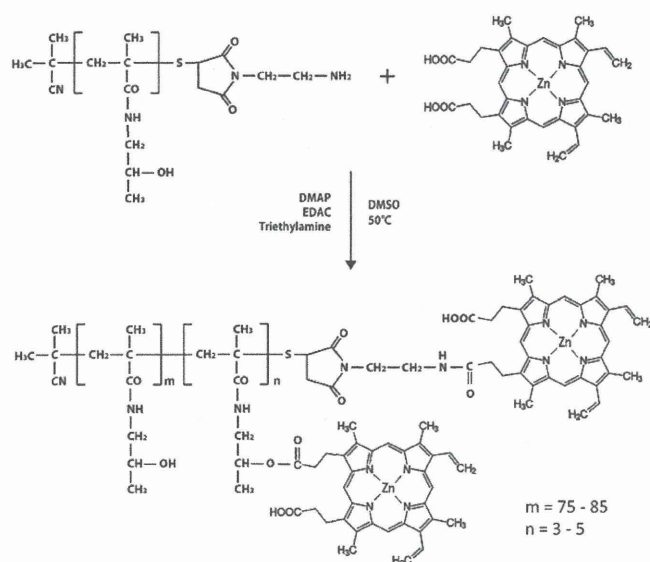
Scheme 1. HPMA-ZnPP synthesis. Chemical structures and conjugation pathway. ZnPP was conjugated to the secondary hydroxyl group and the terminal amino group of HPMA.

HPMA-ZnPP were analyzed by using a transmission electron microscope (Tecnai F20; FEI, Hillsboro, OR).

2.8. Electron spin resonance (ESR) spectroscopy

ESR spectra were measured by using an ESR spectrometer at 25 °C (JES FA-100; JEOL, Tokyo). Sample solutions containing 200 μg/ml HPMA-ZnPP (or 40 μg/ml ZnPP) and 20 mM 4-oxo-TEMP with or without light irradiation were evaluated. Samples in a flat quartz cell (Labotec, Tokyo) were irradiated (28 mW/cm^2) by using xenon light at 400–800 nm (MAX-303; Asahi Spectra, Tokyo) for indicated times. The ESR spectrometer was usually set at a microwave power of 1.0 mW, amplitude of 100-kHz and field modulation width of 0.1 mT.

2.9. Cytotoxicity assay

HeLa cells were maintained in DMEM supplemented with 10% fetal calf serum under 5% CO_2/air at 37 °C. HPMA-ZnPP or ZnPP was added 24 h after plating HeLa cells at 3000 per well in 96-well plates. Irradiation with fluorescent blue light having peak emission at 420 nm (TL-D; Philips, Eindhoven, Netherland) with 1.0 J/cm^2 per 15 min was then performed. After 48 h of culture, the MTT assay was carried out to quantify viable cells, with absorbance at 570 nm as described by instruction of the manufacture.

2.10. Intracellular uptake

HPMA-ZnPP or free ZnPP was added at a concentration of 20 μg ZnPP equivalent/ml 48 h after plating HeLa cells at 25,000 cells per well in 24-well plates (1.9 cm^2/well). At indicated time periods, cells were washed with PBS and added with 2 ml ethanol followed by sonication (20 W, 30 s) to extract the HPMA-ZnPP or free ZnPP. Concentration of ZnPP was measured by fluorescence intensity (Ex. 422 nm, Em. 590 nm).

2.11. In vivo antitumor activity

The care and maintenance of animals were undertaken in accordance with the institutional guidelines of the Institutional Animal Care and Use Committee of Sojo University. Mouse sarcoma S-180 cells (2×10^6 cells) were implanted s.c. in the dorsal skin of ddY mice. When tumor reached to diameter of about 5 mm, 15 mg/kg of ZnPP equivalent drugs in saline was injected i.v. Then after 24, 48 and 72 h, tumor was irradiated by xenon light (MAX-303; Asahi Spectra) at 400–800 nm (20 mW/cm^2) for 5 min as described. Tumor volume (mm^3) was calculated as $(W^2 \times L)/2$ by measuring the length (L) and width (W) of the tumor on the dorsal skin.

2.12. Pharmacokinetics and tissue distribution of HPMA-ZnPP

When S-180 tumor in mice with tumor diameter of approximately 10 mm, injected i.v. was 15 mg of ZnPP equivalent per kg of free ZnPP or HPMA-ZnPP. At the indicated times, mice were killed, perfused with physiological saline and dissected, and then tissues were weighed, DMSO (1 ml per 100 mg of tissue) was added, and samples were homogenized and centrifuged (12,000 g, 25 °C, 10 min) to precipitate insoluble tissue debris, and ZnPP and HPMA-ZnPP in the supernatant were quantified by fluorescence intensity (excitation at 422 nm, emission at 590 nm).

2.13. In vivo fluorescence imaging

Tumor-bearing mice as described above were injected with 15 mg of ZnPP (equivalent) per kg i.v. At 24 h after injection, mice were shaved and, under isoflurane gas anesthesia, were subjected to in vivo fluorescence imaging using IVIS XR (Caliper Life Science, Hopkinton, MA) (excitation at 430 ± 15 nm and emission at 695–770 nm). Fluorescent images of each tissue were also observed after dissection.

3. Results

3.1. Synthesis of HPMA-ZnPP

The carboxyl group of ZnPP was conjugated to HPMA at the secondary hydroxyl group and the terminal amino group (Scheme 1). Gel permeation chromatography of the reaction product on Bio-beads column showed that HPMA-ZnPP had a higher molecular weight than free ZnPP, and neither free ZnPP nor decomposition product was detected (Fig. 1A). The total yield was 47% (wt/wt) based on ZnPP. The macromolecular characteristics of HPMA-ZnPP were also examined by fluorescence polarization. The polarization value (P value) of free ZnPP in dimethylformamide (DMF) was 0.0064, whereas that of HPMA-ZnPP was 0.0378, which suggests that HPMA-ZnPP had a higher molecular weight than ZnPP (Fig. 1B). Also HPMA-ZnPP was shown to have good water solubility of more than 30 mg/ml in water. The ZnPP content in HPMA-ZnPP was estimated as 20% (wt/wt) on the basis of absorbance of ZnPP.

3.2. Micellar structure of HPMA-ZnPP

ZnPP is highly hydrophobic and is believed to form aggregates in water by π–π stacking interactions between tetrapyrrole planes. Thus, we anticipated that HPMA-ZnPP would form micellar structures in aqueous solution; namely ZnPP containing head group can form a hydrophobic inner core as clustered head group, and a hydrophilic HPMA chain as tail would form an outer surface layer facing toward water. Fig. 1C shows that either amide or ester bonds between HPMA and ZnPP are stable in DMSO and in alkaline pH (10 mM NaOH) without DMSO, separately. However, alkaline treatment in DMSO efficiently cleaved HPMA-ZnPP since the micellar structure is disintegrated in organic solvent (DMSO), and OH− becomes accessible to ester bond and resulted in hydrolyzes of ester bond and release of free ZnPP. Dynamic light scattering analyses showed that in aqueous solution of HPMA-ZnPP it formed large micelles particles (hydrodynamic diameter: 82.8 ± 41.8 nm), which suggests that HPMA-ZnPP was associated into micelles in aqueous solution, whereas HPMA alone had a hydrodynamic diameter of 5.6 ± 1.9 nm (Fig. 1D). Transmission electron microscopy also showed the micelle size of HPMA-ZnPP as 30–80 nm (Fig. 1E). HPMA-ZnPP micelles in phosphate-buffered saline (PBS) showed almost neutral zeta potential (+ 1.12 mV).

3.3. HPMA-ZnPP formed micelles via hydrophobic interaction

ZnPP has a λ_{max} at 422 nm in organic solvents such as DMSO and ethanol, and it exists as monodispersed free molecules. However, when free ZnPP molecules aggregate with each other in soluble form in aqueous solution, the λ_{max} shifts towards a shorter wavelength (390 nm). This blue shift was also observed when HPMA-ZnPP was dissolved in aqueous solution (Fig. 1F). Furthermore, the blue shift decreased after adding detergent or Tween 20, or when dissolved in DMSO, but not in the presence of 9 M urea (Fig. 1F). Measurement of fluorescence intensity of HPMA-ZnPP revealed the same phenomenon; HPMA-ZnPP fluorescence was quenched in aqueous solution, which indicates a hydrophobic interaction among aromatic rings or π–π stacking of ZnPP, whereas HPMA-ZnPP fluorescence intensity was restored by adding detergent but not 9 M urea (Fig. 1G, H).

3.4. Demonstration of $^1O_2$ generation from HPMA-ZnPP

The $^1O_2$-generating capacity of HPMA-ZnPP was examined by means of ESR spectroscopy with the use of spin-trapping agent
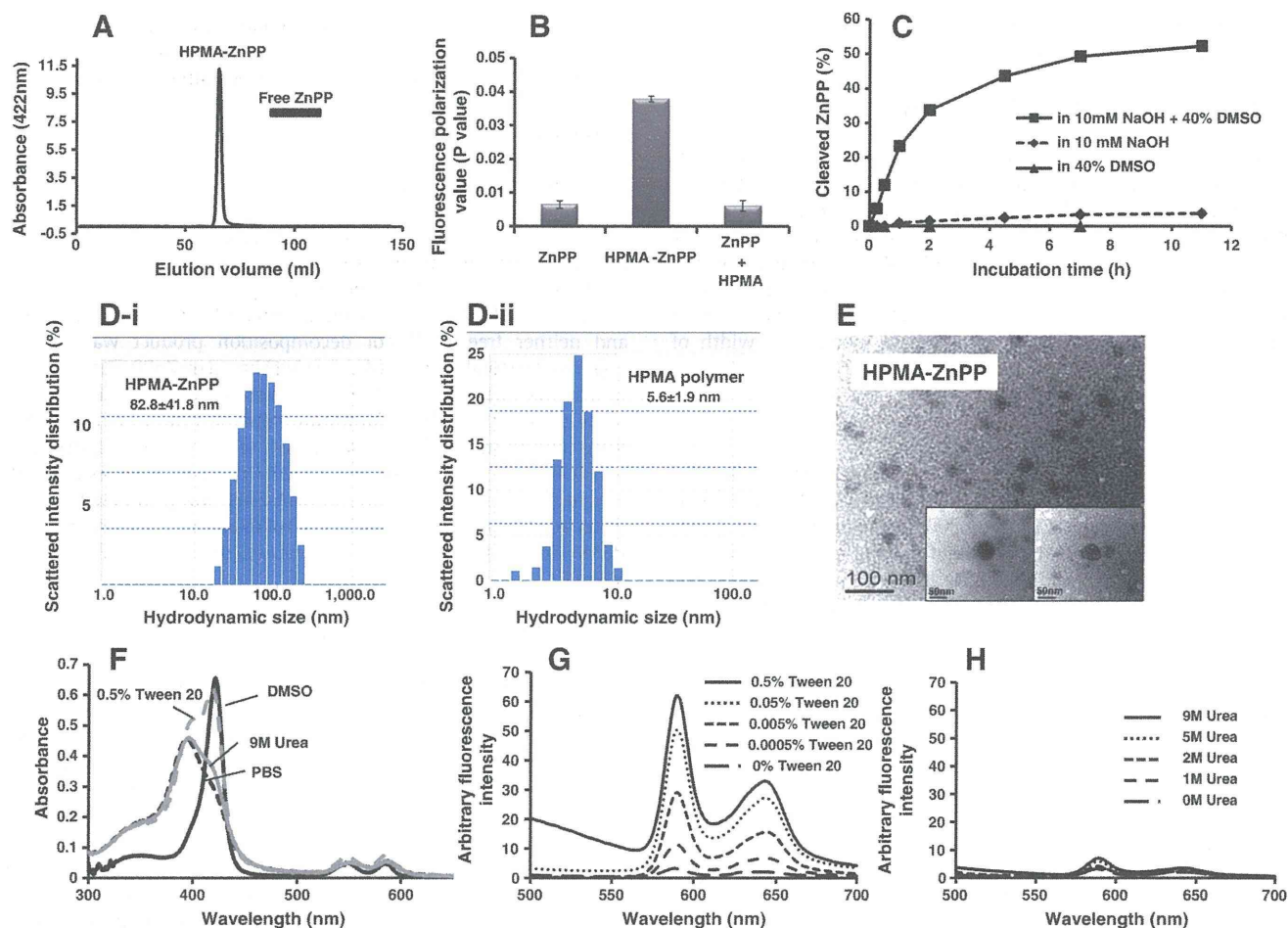
Fig. 1. Properties of HPMA-ZnPP in an organic solvent and aqueous solution. (A) HPMA-ZnPP at 1 or 0.2 mg/ml ZnPP was applied to a Bio-Beads S-X1 column and eluted by DMF, and detected by absorption at 422 nm. The dark bar shows the position of elution of free ZnPP. (B) Fluorescence polarization of ZnPP at 0.5 μg/ml equivalent of HPMA-ZnPP and free ZnPP (with or without addition of 2 μg/ml of HPMA). Fluorescence polarization (P) values were measured (Ex. 420 nm; Em. 590 nm). See text for calculation. (C) Cleavability of HPMA-ZnPP (2.5 mg/ml) dissolved in 10 mM NaOH with or without 40% DMSO at 50 °C was examined. Cleaved free ZnPP was measured by HPLC detected by absorption at 422 nm. (D) The apparent hydrodynamic diameter of HPMA-ZnPP micelles or parental HPMA was measured by using dynamic light scattering. HPMA-ZnPP micelles (D-i) or parental HPMA polymer (D-ii) was dissolved in PBS (pH 7.4) at a concentration of 1 mg/ml. (E) Transmission electron micrograph of HPMA-ZnPP. The micelle image and HPMA-ZnPP size were analyzed via transmission electron microscopy. The inset shows high magnification image. See text for detail. (F) UV/VIS absorption spectra of HPMA-ZnPP dissolved in DMSO or PBS containing 9 M urea or 0.5% of Tween 20. (G), (H) Fluorescence spectra of 10 μg/ml HPMA-ZnPP in the presence of various concentration of Tween 20 (G), or Urea (H).

2,2,6,6-tetramethyl-4-piperidone (4-oxo-TEMP) and light-irradiation. We measured the difference in $^1O_2$ generation in both micellar and disintegrated HPMA-ZnPP forms. When micellar HPMA-ZnPP was dissolved together with 20 mM 4-oxo-TEMP in PBS (pH 7.4) and light-irradiated, it generated no $^1O_2$ (Fig. 2A). However, in the presence of 0.5% Tween 20, its $^1O_2$ generating capacity was observed, where HPMA-ZnPP is disintegrated (Fig. 2A). Addition of sodium azide, a $^1O_2$ scavenger, clearly suppressed the triplet signal of 4-oxo-TEMPO (the $^1O_2$-4-oxo-TEMP adduct) (data not shown). These results agree with those of fluorescence spectroscopy and quenching of HPMA-ZnPP micelles in PBS or aqueous systems (Fig. 1G). Free ZnPP showed a similar character to HPMA-ZnPP micelles, indicating that free ZnPP will aggregate and π–π stacking will be formed in aqueous solution, which contributes to the suppression of singlet oxygen upon light-irradiation (Fig. 2B).

3.5. Cytotoxicity of HPMA-ZnPP

Free ZnPP had an IC$_{50}$ value of about 10 μg/ml, whereas that of HPMA-ZnPP micelles was more than 100 μg/ml of ZnPP equivalent (Fig. 2B). However, with light irradiation, both free ZnPP and HPMA-

ZnPP conjugates showed markedly increased cytotoxicity; 1.0 J/cm^2 light (blue fluorescent light; Philips, Eindhoven, Netherland) with an irradiation peak at 420 nm enhanced both cytotoxicity 10–20 times {(free ZnPP, IC$_{50}$<1.0 μg/ml) and (HPMA-ZnPP, IC$_{50}$ to 5 μg/ml)} (Fig. 2B).

We then examined that the contribution of cytotoxic effect of HPMA-ZnPP induced by light-irradiation is attributable to whether intracellular or extracellular drugs. In one set of assay, light irradiation was applied without a medium change, so that the drug was accessible from outside the cells; in another set of assay, we changed the medium to fresh medium without the drug, so that the drug existed primarily inside the cells. The results showed that medium replacement without the drug caused a slight decrease in cytotoxicity (Fig. 2C), which suggests that intracellular uptake of HPMA-ZnPP was the main cause of light irradiation-induced cytotoxicity.

3.6. Stability of HPMA-ZnPP micelles: lecithin induces disintegration of HPMA-ZnPP

As Figs. 1G and 2A show, HPMA-ZnPP in the intact micellar form, demonstrated the least fluorescence, did not generate $^1O_2$. Thus, to